method [15]. Looking at Eq. (1), since exactly at the boundary the mass flow J is always zero (no solute is drained from the boundaries or moves into them), we have that instantaneously the gradient is the steady-state one. As the time progresses, the thickness of the layers adjoining the boundaries where the steady-state gradient is attained gets larger and larger and eventually the whole height of the sample has the same gradient.

The basic hypothesis we want to test is whether during transients, effects are present other than those described by the theory for the steady-state behaviour. In other words, if at a given instant a layer of fluid has a given concentration gradient, is the scattered intensity the same one would expect as if that layer was in steady-state conditions or are there additional effects? If we assume that the former hypothesis is valid, then from a qualitative point of view it is easy to understand why the curves show little change in the rolloff position and exhibit only a variation of the scattered intensity level. We can crudely divide the cell height into regions where we have the (same) steady-state gradient and regions where the gradient is zero. Then things would make sense, since the rolloff is dictated by the magnitude of the gradient (which as we said is the same), while the intensity is actually controlled by the height over which the steady gradient is attained, and this grows as a function of time, until it eventually attains a terminal, steady-state value.

Let us see if we can test the hypothesis above on a more quantitative basis. We can estimate the scattered intensity by assuming that the overall effect is the sum of the contributions, layer by layer, taking into account the various gradients in the layers as described by Eq. (6), the calculation being carried out as a function of time. We have to integrate Eq. (3) between the boundaries. When that is done, we find that asymptotically the value of the scattered intensity extrapolated at zero q vectors should behave as an exponential:

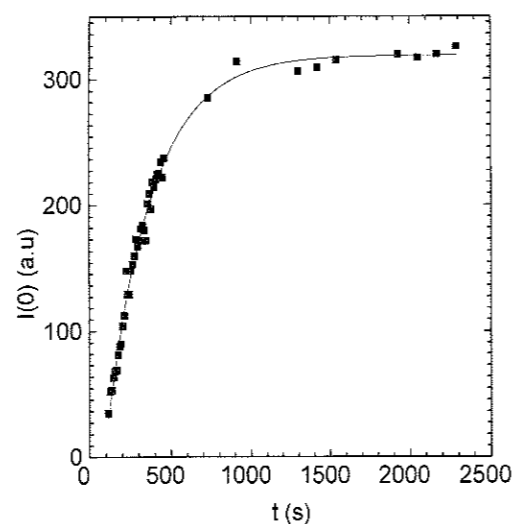$$I(0) = c(0) - c(a) \propto 1 - \exp\left(-\frac{a^2}{\pi^2 D} t\right).$$ (8)

Fig. 4 Time evolution of the nonequilibrium forward scattered intensity. The solid line is the best fit of the data with Eq. (8)

When the actual data for this quantity are plotted as a function of time, a fairly good fit with an exponential is obtained (see Fig. 4). The experimentally derived estimate for the diffusion coefficient D that appears in Eq. (8) turns out to be $D = 3.6 \times 10^{-6}$ cm^2/s to be compared with the estimated value from literature data $D = 1.3 \times 10^{-6}$ cm^2/s [13]. We consider the agreement as fair, since there are so many approximations, especially those stemming from neglecting the concentration and temperature dependence of D and k_T over the cell height.

In conclusion, the preliminary data we present here on time-dependent nonequilibrium fluctuations indicate that no additional effects other than those associated to the presence of a stress induced gradient and described by the steady-state theory are present.

References

1. Law BM, Gammon RW, Sengers JV (1988) Phys Rev Lett 60:1554
2. Law BM, Segrè PN, Gammon RW, Sengers JV (1990) Phys Rev A 41:816
3. Segrè PN, Gammon RW, Sengers JV, Law BM (1992) Phys Rev A 45:714
4. Segrè PN, Gammon RW, Sengers JV (1993) Phys Rev E 47:1026
5. Li WB, Segrè PN, Gammon RW, Sengers JV (1994) Physica A 204:399
6. Segrè PN, Schmitz R, Sengers JV (1993) Physica A 195:31
7. Segrè PN, Sengers JV (1993) Physica A 198:46
8. Vailati A, Giglio M (1996) Phys Rev Lett 77:1484
9. Carpineti M, Ferri F, Giglio M, Paganini E, Perini U (1990) Phys Rev A 42:7347
10. Vailati A, Giglio M, to be submitted
11. Calmettes P, Lagues I, Laj C (1972) Phys Rev Lett 28:478
12. de Groot SR, Mazur P (1962) Nonequilibrium Thermodynamics. North-Holland Amsterdam
13. Giglio M, Vendramini A (1975) Phys Rev 34:561
14. Bierlein JA (1955) J Chem Phys 23:10
15. Tanford C (1961) Physical Chemistry of Macromolecules. Wiley, New York

H. Löwen
M. Schmidt

Freezing in confined suspensions

H. Löwen[1] (✉) · M. Schmidt
Institut für Theoretische Physik II
Heinrich-Heine-Universität Düsseldorf
Universitätsstraße 1
40225 Düsseldorf, Germany

[1] also at:
Institut für Festkörperforschung
Forschungszentrum Jülich
52425 Jülich, Germany

Abstract The freezing transition of hard sphere colloids confined between two parallel hard plates is studied for different plate distances ranging from one to two particle diameters. Using Monte Carlo simulations and free volume theory, the full phase diagram is obtained exhibiting solid-to-solid transitions between buckled, rhombic and layered crystals involving several triangular or square layers. While the fluid freezing transition is always strongly first order, both strong and extremely weak transitions occur between different crystalline structures. These predictions should be experimentally observable in confined suspensions of sterically stabilized or highly salted charge-stabilized colloidal particles.

Key words Confined fluids – freezing transitions – colloidal suspensions

Introduction

If a fluid is confined on a microscopic scale, the location of its phase transitions can be significantly shifted with respect to that of the bulk system. While this effect is well-known and well-studied for the liquid-vapour transition [1] where capillary condensation can stabilize the liquid phase at the expense of the gas it is much less clear how the freezing transition is affected by a confinement. Recent studies indicate [2, 3] that the direction of the shift of the fluid freezing line depends delicately on the range and nature of the wall–fluid interaction. Another significant shift is expected for the (dynamical) glass transition in a confined system, see e.g. Ref. [4] for a computer simulation study and a compilation of literature.

Different kinds of confinement are conceivable: the liquids can be inside a porous material (like vycor glass or silica gels), inside a spherical or cylindrical cavity or in between two parallel smooth plates. In the following we shall mainly study a system confined between two parallel walls but we add also some qualitative remarks for other confinements. In between two walls, the effective dimensionality of the confined fluid may be continuously interpolated between three and two by varying the plate distance from macroscopic towards molecular spacings. This may also help to explain why the freezing transition in such a confining geometry is difficult to understand: In strictly three- or two-dimensional fluids it was found that the freezing and melting transition can be quite different. While it is a usual first-order transition in 3D, it may be a two-stage continuous transition in 2D with an intermediate hexatic phase possessing long-ranged bond-orientational order [5]. Hence it is a priori unclear which of these two situations is realized in between two and three dimensions although there are certain indications that an intermediate phase can persist between two and three dimensions provided it occurs in the pure 2D case. The orientational symmetry of such an intermediate phase may be sixfold ("hexatic phase") as well as fourfold ("tetratic phase"), threefold ("triatic phase") or twofold ("duatic phase").

Colloidal suspensions represent excellent model liquids on a mesoscopic length scale. They possess many

advantages over molecular (microscopic) liquids: First, they can be easily confined between parallel glass plates. On a mesoscopic scale these plates are much smoother than in any confinement of microscopic fluids. The larger size of colloidal spheres allows one to watch their positions in real space using video microscopy, see e.g. Refs. [6–13]. What is known from this work is that many different crystalline phases can become stable as one varies the plate separation. In the experimental work [7], the following cascade of solid-to-solid transitions was found

$$... n\triangle \rightarrow (n+1)\square \rightarrow (n+1)\triangle ... . \qquad (1)$$

This implies an alternation of crystals involving n square layers ($\square$) with crystals consisting of $n+1$ layers of stacked two-dimensional triangular lattices ($\triangle$).

Theoretical work, on the other hand, is much less comprehensive and was mainly done in the framework of a hard-sphere model confined between hard walls: Pieranski and coworkers have calculated the close packing density [14] and used a cell model to calculate some solid-to-solid transitions [15]. The structure of the confined hard sphere fluid was investigated by Percus [16] and Wertheim et al. [17] without addressing the freezing transition. Finally, within a Landau approach, a transition from a crystalline monolayer to buckled solid phase was recently pointed out by Chou and Nelson [18].

In this paper we present calculations of the full phase diagram for the confined hard-sphere model for arbitrary density and moderate plate distances lying between one and two sphere diameters. The phase diagram exhibits a rich structure with a fluid phase and many different solid phases including buckled, rhombic and layered crystalline structures. We find that the sequence (1) suggested by the experiments is in fact more complicated since additional buckled and rhombic phases may also occur. We have also addressed the question after the order of the solid-to-solid transitions. In fact they can be strongly first order as well as very weakly first order. The results are obtained using extensive Monte Carlo (MC) simulations. We also present a simple theory for the phase diagram, combining free volume theory of the crystalline phase with an effective-diameter theory of the fluid phase, which yields qualitative and semi-quantitative agreement with our exact simulation data. At least for our model studied we do not find an indication for an intermediate phase with algebraically decaying bond-orientational order. A part of this work has been published already elsewhere [19].

The paper is organized as follows: In the second section we propose and define our model. Then we describe our Monte-Carlo simulation technique in the third section. Then, in the fourth section, we summarize our results and discuss our simple theory in terms of a cell model in the fifth section. We conclude in the sixth section. One peculiar

emphasis of our paper is to give a survey on other possible fascinating transitions in confining geometry. This is finally done in the seventh section.

The model: hard spheres between hard plates

Our model consists of N hard spheres of diameter σ confined between parallel hard plates with area A and gap thickness $H = (h+1)\sigma$, such that $h = 0$ corresponds to the 2D limit of hard disks. Since temperature is irrelevant for excluded-volume interactions, the only thermodynamic quantities are the reduced particle density $\rho_H = N\sigma^3/(AH)$ and the effective reduced plate separation h. The particle coordinate perpendicular to the plates is z, with $-h\sigma/2 \leq z \leq h\sigma/2$. In the limit $h \rightarrow \infty$, the effect of the confining plates vanishes and the 3D bulk hard sphere system is recovered.

Monte-Carlo simulation

In our Monte-Carlo simulations, we use the canonical ensemble with particle numbers ranging from $N = 192$ to $N = 4608$ in order to check systematically for finite-size effects. Careful attention is paid to the boundary conditions, which are crucial in a system exhibiting structural phase transitions. To allow any periodically ordered structure to fit into the simulation box for a suitable particle number N, the box is allowed to change its shape in the course of the simulation while its volume is fixed. The area in the lateral plane is a parallelogram with periodic boundary conditions. MC moves concerning its angles and aspect ratio are performed, so that the system can relax to equilibrium via shearing and squeezing. Between 10 and 100 million MC steps per particle were computed to determine the equation of state for fixed h in the region of a phase transition. Phase transitions are detected by looking for van der Waals loops in the equation of state for fixed h. By performing a Maxwell construction, the corresponding density jump is calculated by equating both the lateral pressures $p_{lat} = -H^{-1}\mathrm{d}F/\mathrm{d}A$ (F denoting the Helmholtz free energy) and the chemical potentials of the coexisting phases. As a consistency check, we have also used the single occupancy cell method [20] for $h = 0.85$ finding the same phase boundaries. In addition, we have monitored the behavior of suitably defined order parameters in order to characterize the emerging crystalline phases. We introduce a set of double-indexed complex order parameters Ψ_{mn}, defined via

$$\Psi_{mn} \equiv \left\langle N^{-1} \sum_{\alpha=1}^{N} |\Psi_n(\alpha)| \exp(im \arg \Psi_n(\alpha)) \right\rangle . \qquad (2)$$

Here $\langle ... \rangle$ denotes a canonical average and $\Psi_n(\alpha) \equiv N_\alpha^{-1}\sum_\beta \exp(in\Theta_{\alpha\beta})$, where the sum is over N_α neighbours of particle α possessing lateral distances smaller than 1.2σ and having opposite signs in their z-coordinates and $\Theta_{\alpha\beta}$ is the angle between the bond of particles α and β and an arbitrary axis. The quantity Ψ_{mn} tests for solid structures with an $m \cdot n$-fold rotational symmetry. By calculating the order parameter set $\{\Psi_{mn}\}$ during the simulation, one can readily distinguish between different local surroundings of particles and thus identify the crystalline structure. An abrupt change in the order parameters signals a phase transition. The fluctuations of the order parameters are measured by means of an order parameter susceptibility

$$\chi_{mn}(N) = N(\langle |\Psi_{mn}|^2 \rangle - \langle |\Psi_{mn}| \rangle^2) ,$$

depending on the particle number N. It will be used to investigate the order of weak phase transitions. (The dependence of Ψ_{mn} and χ_{mn} on the thermodynamic variables ρ_H and h is suppressed in the notation.) The following two scenarios are conceivable: In the case of a continuous phase transition, diverging fluctuations are observed at the critical point, and $\chi_{mn}(\rho_H \rightarrow \rho_H^{crit}) \rightarrow \infty$. Of course, diverging fluctuations are only encountered in the thermodynamic limit $N \rightarrow \infty$, which is not directly accessible in computer simulations. Hence we study the dependence of χ_{mn} on the system size N. In the discontinuous case, on the other hand, entering the coexistence region would simply mix the susceptibilities of the coexisting phases according to the relative weight of both phases $\chi_{mn}(\rho_H) = \alpha\chi_{mn}(\rho_H^{(1)}) + (1 - \alpha)\chi_{mn}(\rho_H^{(2)})$, $\alpha = (\rho_H^{(1)}/\rho_H)(\rho_H^{(2)} - \rho_H)/(\rho_H^{(2)} - \rho_H^{(1)})$, (here the superscripts 1 and 2 stand for the low- and high-density coexisting phases). Consequently, no divergence is encountered as $N \rightarrow \infty$.

Results

In Fig. 1, the resulting phase diagram is shown in the plane spanned by the reduced particle density ρ_H and the effective plate spacing h. The region in phase space is naturally limited by the close-packed density (dashed line). Different symbols represent different system sizes showing that the dependence on system size is only weak. For $h = 0$, in agreement with recent simulations of Weber et al. [21], we recover the first-order freezing transition of hard disks into a triangular lattice. As h is increased, the fluid freezes first into one triangular layer and with increasing density subsequently undergoes a further first-order transition into a crystalline structure of buckled lines (b). For intermediate h, the fluid freezes into two layers of a square lattice ($2\square$) via a strong first-order transition and then transforms into the buckling phase (b). The latter transition is marked by $\triangle$-symbols indicating phase boundaries, where the
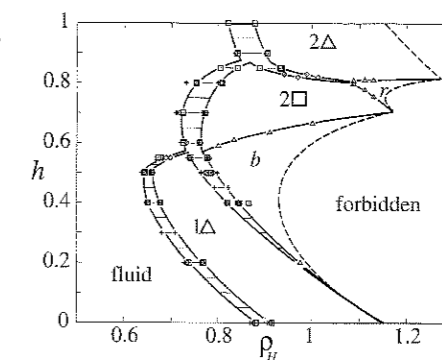

Fig. 1 Simulated phase diagram for hard spheres of reduced density ρ_H between parallel plates with effective reduced distance h. Symbols indicate different system sizes: $N = 192$ (+); $N = 384$, 512 (◇); $N = 576$ (△); $N = 1024$, 1156 (□). Six phases occur (fluid, $1\triangle$, b, $2\square$, r and $2\triangle$). The closed-packed density is marked by a dashed line. Solid lines are guides to the eye. Thin horizontal lines represent two-phase coexistence

equation of state shows no van der Waals loop, but the order parameter Ψ_{21} exhibits anomalous behaviour. The order parameter Ψ_{21} is shown in Fig. 2 for fixed plate separation distance $h = 0.62$ as a function of density ρ_H. The function $\Psi_{21}(\rho_H)$ increases in a relative small density interval $\rho_H = 0.87 - 0.9$ from a value close to zero to a finite value of about 0.04. We find that the fluctuations on the low-density side vanish with a law $\propto 1/\sqrt{N}$ and tend to zero in the thermodynamic limit $N \rightarrow \infty$. We thus conclude, that the $2\square$-phase is thermodynamically stable for low densities. In contrast, on the high-density side, no decrease of Ψ_{21} as a function of particle number N is observed; from the finite-size systems' data we can conclude that a value clearly larger than zero is reached as $N \rightarrow \infty$, and the buckling structure with only two-fold rotational symmetry is stable. We thus conclude that a phase transition happens between $2\square$ and b, signalled by a rapid increase of the order parameter Ψ_{21} as a function of density ρ_H. As a function of N, the increase happens more rapidly (with a larger slope) and is shifted towards higher densities.

Having demonstrated the existence of $2\square-b$ phase transition, we are now concerned with its order. Therefore the order parameter susceptibility is considered. In Fig. 3 the susceptibility χ_{21} as a function of density ρ_H is shown for plate separation distance $h = 0.62$. The susceptibility has small, but finite values in the low-density $2\square$- and high-density buckling phase. In between the pure phases a pronounced maximum occurs that can be interpreted in terms of fluctuations driving the system from one phase to the other. In contrast to the finite-size dependence of the order parameter itself, its susceptibility shows only weak dependence on system size. Although statistical errors are present, there is no indication up to $N = 4608$ of a
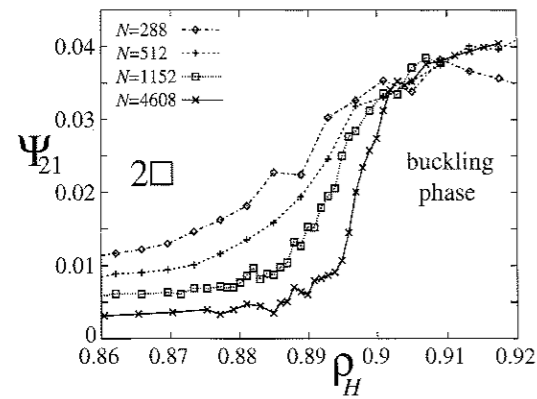
Fig. 2 Behaviour of the order parameter Ψ_{21} across the $2\square$–b phase boundary as a function of density ρ_H for plate separation distance $h = 0.62$. There are four different system sizes shown $N = 288, 512, 1152, 4608$
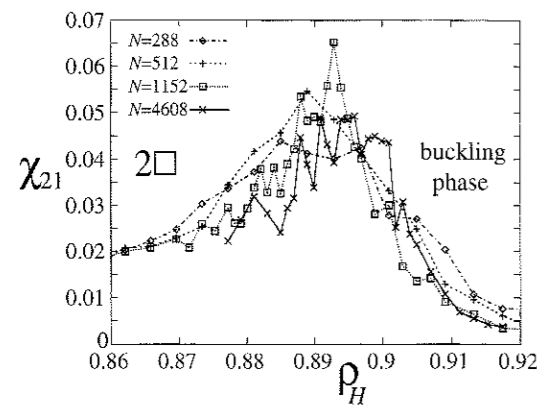

Fig. 3 Finite-size dependence of the order parameter susceptibility χ_{21} for particle numbers $N = 288, 512, 1152, 4608$ and plate separation $h = 0.62$. The maximum of the curves remains finite as a function of N

divergence in the thermodynamic limit. We thus conclude, that although we cannot resolve a probably miniscule density jump from the equation of state, the phase transition between the $2\square$ and the buckling structure is of first order. However, for $h = 0.6$, for example, we can exclude a density jump $\Delta\rho_H$ larger than 0.0004. Hence the $2\square \to b$ transition is extremely weak.

For even higher h, a transition occurs from the $2\square$ phase into a crystal with two triangular layers ($2\triangle$). Finally there is a new stable crystalline phase which we call rhombic (r) since its unit cell is a rhombus. It is a close-packed structure but its stability also extended towards slightly smaller densities. The $2\square \to r$ and $2\triangle \to r$ transitions are again very weak.

Let us add some more details for the two less common phases b and r. Typical particle configurations and the corresponding unit cells are depicted in Figs. 4a and b.
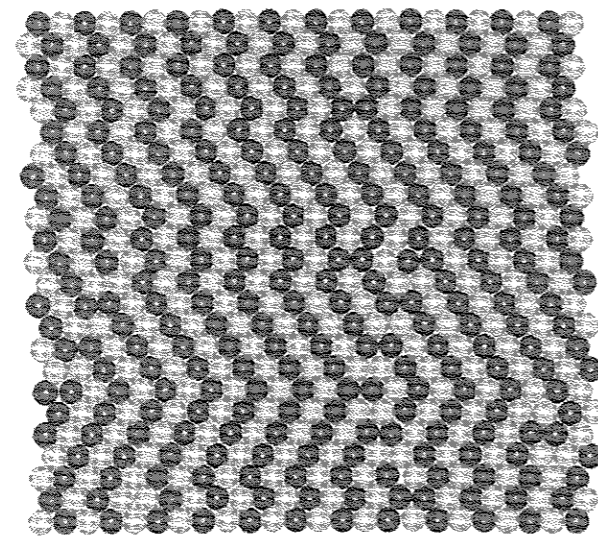
(a)
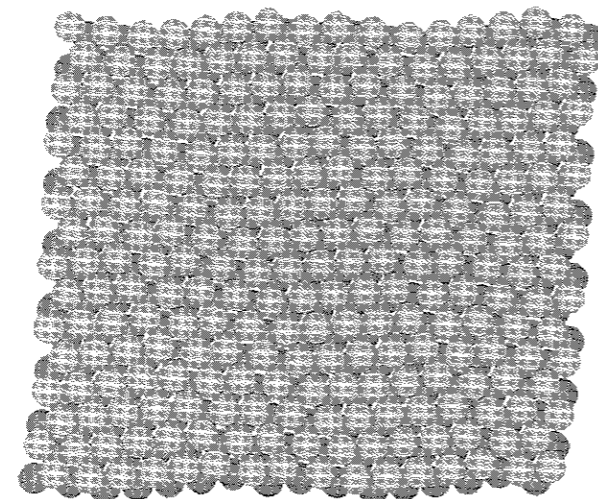
(b)

Fig. 4 Typical configurations of (a) the buckling phase, and (b) the rhombic phase

Both structures possess twofold rotational symmetry. Interestingly enough both the buckling and the rhombic phase are *highly degenerate*. For the buckling phasely, there is linear buckling (constituted by a single rectangular unit cell), periodic zig-zag buckling (built up from left and right kites) and a random succession of both (shown in Fig. 4a). Still, in the horizontal direction, there is strict periodicity. Likewise, the rhombic phase can appear to be linear rhombic (with a single rhombic elementary cell), zig-zag rhombic (with an alternating succession of the two rhombi) and again a radom succession of both as shown in Fig. 4b. All of these structures are close packed at the corresponding values of h. Away from close packing we

cannot distinguish within our simulation which of these phases is the thermodynamically stable one since the free-energy differences are too miniscule. Let us remark that this is quite similar to the 3D hard-sphere crystal, where the three close-packed structures fcc, hcp, and random stacking are extremely close in free energy and the actual crystalline structure depends on the history of the sample.

We emphasize that the fluid freezing transition is first order. In fact we checked that bond-angle orientational correlation functions with two-, four- and six-fold symmetry decay exponentially with distance in the fluid phase and reach a finite plateau value in the solid phase. At least for a system size of $N \leq 1156$, we never found an intermediate "duatic", "tetratic" or "hexatic" phase characterized by an algebraic decay of the corresponding orientational correlation. This fact, of course, does not exclude the occurrence of such phases in larger systems and in systems that are governed by softer interactions.

Free volume theory

Cell model for crystalline phases

The cell model exploits the physical picture of a solid with particles being located around given lattice sites [15, 22, 23]. It enables one to determine the thermodynamically stable crystalline structure and its equation of state approximately. Furthermore, it provides an exact upper bound on the free energy.

In principle, the theoretical problem of hard spheres in confined geometry consists of computation of the configurational integral over N 3D spatial coordinates, the integrand being the Boltzmann factor, which is in the case of hard bodies either unity for allowed configurations or zero if at least two particles overlap. Adopting the cell model, we first impose a candidate lattice structure with given average density ρ_H and plate separation H. In general, this structure will depend on a set of free geometric parameters $\{a_i\}$, e.g. angles, ratios of lattice constants, etc. Second, the integration regime of each particle in the configurational integral is restricted from the total volume V to a smaller region in space around each lattice site, called the free volume cell. Thereby the cell size is chosen small enough, so that any two neighbouring spheres restricted within their respective cells cannot penetrate each other, hence the integrand of the restricted configurational integral is unity, the N integrals decouple and yield v_f^N, where v_f is the spatial volume of one cell. Clearly, the expression $-k_BT \ln(v_f/\Lambda^3)$ provides an upper bound on the exact (Helmholtz) free energy per particle, Λ denoting the thermal de Broglie wave length. To optimize this bound, we minimize it with respect to the set of free parameters $\{a_i\}$.

We checked the available analytical expression for v_f for the $1\triangle$-, b-, $2\square$-phases against an exact numerical procedure [24]. A modification is done for the $1\triangle$-phase [15] where we inserted a different effective diameter $\sigma^*_{1\triangle} = \sigma\sqrt{1 - h^2/6}$ into the expression for the $1\triangle$-free volume in order to enlarge the free volume for two touching spheres with different z-coordinates.

As the deviation of the cell model result from the exact free energy is expected to depend only weakly on the explicit crystal structure, and only free energy *differences* enter in the calculation of the phase diagram, phase boundaries between different crystalline phases are expected to be reasonably reproduced within the cell model.

Effective-diameter fluid theory

The fluid in slab geometry is approximately treated as a strictly two-dimensional hard-disk system with an effective diameter σ^* obtained from the implicit relation

$$\sigma^{*2} = \sigma^2 - \int_{-h\sigma/2}^{h\sigma/2} dz_1 \int_{-h\sigma/2}^{h\sigma/2} dz_2 (z_1 - z_2)^2 \, \rho(z_1, \sigma^*)$$
$$\times \rho(z_2, \sigma^*)/(\rho_H(h + 1)\sigma^{-2})^2 \qquad (3)$$

where the one-particle density profile $\rho(z, \sigma^*)$ is given by $\rho_H(h + 1)\exp(\alpha(\sigma^*)z^2)/\mathcal{N}(\alpha(\sigma^*))$ with the normalization $\mathcal{N}(\alpha) = \sqrt{\pi/\alpha}\sigma^2 \, \mathrm{erfi}(\sqrt{\alpha}h\sigma/2)$ and $\alpha(\sigma^*) = \pi\rho_H(h + 1)g(\sigma^*)/\sigma^2$, $\mathrm{erfi}(x)$ denoting the imaginary error function. Here, $g(\sigma^*) = (1 - \eta(\sigma^*)/2)/(1 - \eta(\sigma^*))^2$ is the contact value of the 2D pair correlation function within scaled particle theory, and $\eta(\sigma^*) = (\pi/4)\rho_H(h + 1)\sigma^{*2}/\sigma^2$ is the effective area fraction of the 2D system. The expression (3) takes into account the fact that two spheres can be laterally closer than σ if they differ in their z-coordinates. Finally the Helmholtz free energy is obtained via integration of $dF/dA = -k_BT\rho_H(1 + h)(1 + \pi\rho_H(h + 1)\sigma^{*2}g(\sigma^*)/2\sigma^2)/\sigma^2$ guaranteeing the correct second virial coefficient in the low-density limit. The integration constant F_0 is empirically chosen to fit the location of the hard-disk freezing transition.

Phase diagram

The theoretical phase diagram is shown in Fig. 5. It looks similar to the exact simulation data reproducing the stability of the six different phases found in the simulation. All transitions are first order. The density gap between $b \to 2\square$ and $r \to 2\triangle$ is extremely small, for instance, $\Delta\rho_H = 0.00047$ at $h = 0.72$ for the $b \to 2\square$ transition. Also the fluid $\to 1\triangle$ and $1\triangle \to b$ transitions are quantitatively correct. Another interesting property concerns the above-mentioned
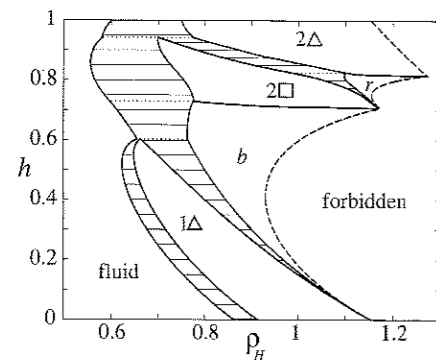
Fig. 5 Same as Fig. 1 but now obtained from effective-diameter and cell theory. The dotted lines represent a situation with three coexisting phases

degeneracy of the b and r phases. Indeed, also away from close packing, the free volumes are identical for different realizations of the b and r phases and hence the cell model cannot distinguish between the subspecies. One can thus conclude that the cell model, which requires much less numerical effort than a direct simulation, gives reliable results as far as the topology of the phase diagram of confined hard-body systems is concerned. Some details of the phase diagram, however, are not reproduced. The slope of the $2\square \to b$ line is positive in simulation but negative in cell theory. Hence the cell theory overestimates the stability of the buckled phase. Furthermore, the agreement of the fluid–solid coexistence region grows worse as h increases since within effective-diameter theory we map a multi-layer fluid onto a single-layer fluid.

Conclusions

In conclusion we have calculated the phase diagram of hard spheres confined between two parallel hard plates for small plate distances H ranging from one to two sphere diameters. Although solely excluded volume interactions enter in our model, it may also be used for softer interactions as long as they can be mapped onto an effective hard sphere system confined between effective hard plates. The interaction of a charged suspension is Yukawa-like [25–28] but image charges are also important if the dielectric constant of the solvent and the confining plates differ [25]. The screening length decreases with increasing salt concentration of the solvent. Therefore a charged suspension between charged plates could be mapped onto an effective hard-sphere system if the salt content is high. However, one should be careful in details of the freezing transition as far as an intermediate phase is concerned. It is known that the softness of a pretty harsh interaction $\propto r^{-12}$ is already sufficient to produce an intermediate

hexatic phase in 2D [29, 30] which is absent for hard disks [21].

An experimental verification of the full phase diagram is highly desirable in confined sterically stabilized colloidal suspensions or in charged but highly salted dispersions. Using video microscopy or scattering methods one should be able to resolve the order of the solid–solid transitions in order to verify our predictions. Let us also mention that similar solid-to-solid transitions were recently found [31, 32] for bilayer Wigner crystals in a double-quantum-well system exposed to a strong magnetic field.

Outlook and open problems

There are still many related questions open which we summarize in the following:

Larger plate distances: multilayer systems

The first problem obviously concerns the extension of our results to larger plate separations H. Here the situation becomes more and more complicated due to two reasons. First there are much more structures conceivable in packing spheres between larger spaced plates. Second all these phases compete in free energy and the free energy differences can become tiny. Hence it is difficult and practically impossible to resolve these small differences by a computer simulation. For a multilayer system, only the location of the fluid–solid transition has been simulated [33] without resolving the different solid phases. What is also known is that for infinite plate separation a layer of finite thickness of the metastable bulk crystal covers the plates. This precrystallization effect was demonstrated by van Swol and coworkers [34].

In our work, we have left out any possible transition structure to three layers, which emerge at $H > 1.82\sigma$ for high densities. Even the density of close packing is not known in this case. Recent experiments [11] suggest that again quite exotic structures can be generated in three and more layer systems. For instance, one strongly expects the stability of a "super-buckled phase". This phase consists of straight rows of triangles. In a two-dimensional cut perpendicular to the walls and normal to the row direction, there are alternating triangles of different orientation. Such a phase can be understood by packing Swiss "Toblerone" chocolates into an intersecting buckled structure. The corresponding two-dimensional cut is sketched in Fig. 6. Phases involving more layers can possess an even more exotic structure. After all, the simple sequence (1) is only true for a path well in between the crystal melting density and close-packed density but is not valid in general.
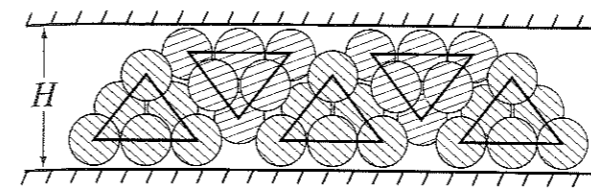

Fig. 6 A sketch of the "Toblerone" structure. The structure is periodic in the direction perpendicular to the drawing plane

Ensemble of constant wall pressure

As a second problem, one can also think in terms of a different thermodynamic ensemble where the pressure perpendicular to the walls is fixed instead of a fixed wall separation H. The choice of the ensemble clearly depends on the kind of experiment one is doing. In the new ensemble of constant wall pressure, the phase transition lines will shift a bit although the overall topology of the phase diagram should not change. However, one should bear in mind that transition between phases belonging to different wall separations are possible. Therefore additional phase transitions are conceivable. One example of these are the so-called stratification transitions found in Ref. [35]. We finally remark that the Gibbs phase rule is not violated in this ensemble since the relative portion of the three coexisting phases is uniquely determined by the wall pressure exerted on the system.

Another complication is the wedge geometry which is actually used in experiments [7]. Only if the relative tilt angle is small one can view the sample as one with parallel plates.

Density functional theory for the phase diagram

The third problem is to do a more sophisticated theoretical treatment involving classical density functional theory of 3D bulk freezing [36]. Many approximations for the free energy density functional which describe 3D bulk freezing are now available. However, most of these approaches suffer from the fact that there are unphysical divergencies if one shrinks the three-dimensional functional towards two dimensions by applying an external potential of two parallel hard walls. This was particularly investigated by Rosenfeld, Tarazona and the present authors [37]. It was found that a geometrically based density functional for hard spheres as originally proposed by Rosenfeld [38] does survive the 2D (and even the 1D and quasi-zero-dimensional) limit. This functional can be modified to describe very accurately the bulk freezing transition of hard spheres [37]. Hence one should take
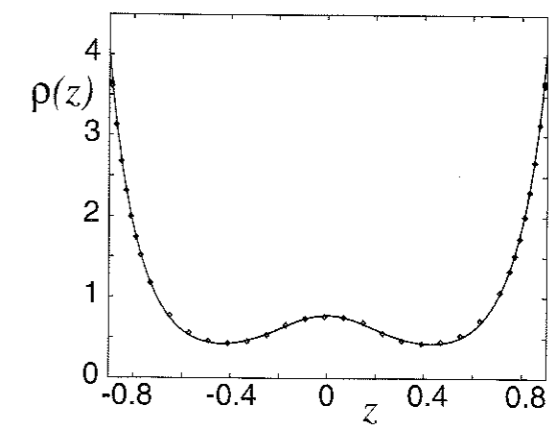

Fig. 7 Density profile of the hard sphere fluid in a planar slit of reduced separation $h = 1.8$. Symbols are Monte-Carlo results, the solid line is predicted by the fundamental-measure free energy density functional [38]

Rosenfeld's functional in order to investigate the phase diagram of hard spheres between hard plates. The problem of density parameterization can be avoided by adopting the free minimization scheme as developed and applied in Ref. [39]. In order to demonstrate the ability of Rosenfeld's functional to describe accurately the density profile we have confronted the density profiles in the fluid phase as resulting from density functional theory with the results from computer simulation, see Fig. 7. The agreement is excellent. One should bear in mind, that theories relying on weighted densities reproducing the direct correlation function in 3D do fail in describing the correct number of maxima in the density profile [40]. This gives a strong indication that Rosenfeld's functional is superior to other approximations, at least in a situation of heavily confined geometry.

Effect of gravity

Real suspensions are not completely density matched, i.e. the mass density of the solvent and that of the colloidal particles differ in general resulting in a non-vanishing buoyant mass M of the colloidal particles. This implies that gravity comes into the game which typically acts normal to the walls and leads to sedimentation. Gravity can be modelled by adding an external potential linear in the z-coordinate perpendicular to the plates. Including gravity, the phase diagram becomes more complicated depending also on the reduced coupling $\alpha \equiv Mg\sigma/k_BT$ where g is the gravitational acceleration.

One may ask whether the complicated superlattice structures found in recent experiments [11] which do not

occur in our "free" phase diagram ($\alpha = 0$) are due to gravity. In order to check this one can study the case $\alpha \to \infty$ implying that gravity becomes dominant. In this case, entropy becomes irrelevant and the stable configuration simply minimizes the gravitational potential energy. Even in this limit, the whole phase diagram depending on h and ρ_H, is not known. It is, however, expected that the typical structure is a phase separation involving dense-packed triangular layers residing on the lower plate with a coexisting part of the close-packed structure at the given H. This statement can at least be proved in the range where the buckled phase is closed packed. This is illustrated in Fig. 8. From this consideration one can conclude that gravity does not induce complicated superstructures. Still results for finite α are missing.

Fig. 8 In the limit of strong gravity g (heavy particles) there occurs a phase separation into triangular layers (left side) and close-packed regions (right side)

Hard cylinders between parallel hard plates

Replacing the hard spheres by hard cylinders or hard spherocylinders one obtains an even more complicated system which can also be realized in the context of colloidal suspensions or microscopic anisotropic fluids [41]. Cylinders carry an additional orientational degree of freedom and the 3D bulk phase diagram involves different mesophases, namely isotropic, nematic, smectic A, plastic crystalline and other crystalline phases [42]. Confining the system by parallel hard plates, the aspect ratio p of the cylinders is an additional parameter (for spheres p is unity). Even the closed-packed density is not known as a function of p and H. There may be a multitude of possible phases which are stable. One interesting phase transition is depicted in Fig. 9 which happens if the plate separation is a bit larger than the length of the cylinders. Then, due to simple packing arguments, a transition occurs from crystalline layers containing cylinders oriented parallel to the walls to one smectic or crystalline layer with rod orientations perpendicular to the walls. This transition is expected to possess a large hysteresis since the structures are completely different.

In order to resolve all these interesting transitions one should perform a simple free volume theory as well as an extensive Monte-Carlo simulation for different aspect ratios p.

Hard spheres in cylindrical and spherical cavities

If the cavity is spherical or cylindrical the kind of transitions are quite different. For a *cylindrical* cavity of fixed diameter, the system is one dimensional. Then the configurations have a helix structure, but there are no phase transitions as the density is varied. Varying the
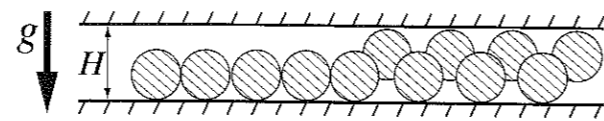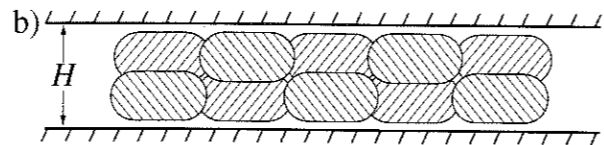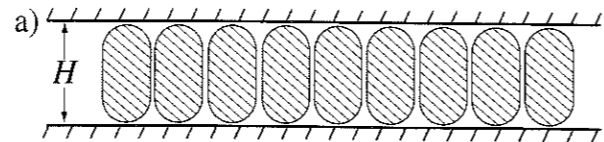

Fig. 9 Two possible phases for hard spherocylinders between parallel plates with plate distance comparable to particle length: (a) one smectic or crystalline layer with rod orientations perpendicular to the walls, (b) two-layered close-packed structure with spherocylinders aligned parallel to the confining walls
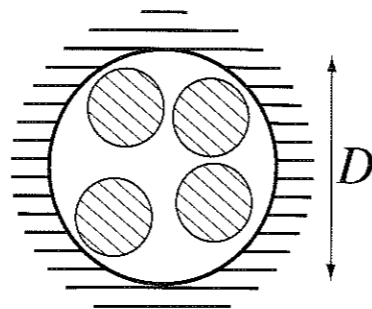

Fig. 10 Four hard spheres confined in a spherical cavity of diameter D

cylinder radius R^*, however, one can reach certain points where an anomalous behaviour can be found; the easiest case is $R^* = \sigma$ which is the border where two neighbouring spheres can exchange their position by hopping over each other. As far as we know, the close-packed density has not yet been calculated for $R^* > \sigma$.

In a *spherical* cavity of diameter D, the number N of hard spheres which can be packed into the big sphere depends crucially on the ratio D/σ, see Fig. 10. The close-packed configuration is a dumb-bell for $N = 2$, a triangle for $N = 3$ and a tetrahedron for $N = 4$. For $N > 4$,

however, this configuration is non-trivial and not yet known. The simpler two-dimensional problem of packing circles into a circle is better understood [43]. Also, recently, computer codes were developed and applied to a similar problem of how to pack two-dimensional circles into a square [44]. The solution for $1 \leq N \leq 20$ was presented in Ref. [44] exhibiting really some unexpected configuration for "odd" numbers N. A similar interesting result should be obtained in three dimensions. These dense-packed configurations should then be observable in porous materials.

References

1. Rowlinson JS, Widom B (1982) Molecular Theory of Capillarity. Clarendon, Oxford
2. Christenson HK (1995) Phys Rev Letters 74:4675
3. Duffy JA, Clarke AP, Fretwell HM, Alam MA, Evans R (1996) J Phys Condens Matter, in press
4. Fehr T, Löwen H (1995) Phys Rev E 52:4016
5. Strandburg KJ (1988) Rev Mod Phys 60:161
6. Pieranski P, Strzelecki L, Pansu B (1983) Phys Rev Lett 50:900
7. Van Winkle DH, Murray CA (1986) Phys Rev A 34:562; Murray CA, Sprenger WO, Wenk RA (1990) Phys Rev B 42:688; Murray CA (1992) In: Strandburg KJ (ed) Bond-orientational Order in Condensed Matter Systems. Springer, New York
8. Weiss J, Oxtoby DW, Grier DG, Murray CA (1995) J Chem Phys 103:1180
9. Schaertl W, Sillescu B (1994) J Stat Phys 77:1007
10. Marcus AH, Lin B, Rice SA (1996) Phys Rev E 53:1765
11. Neser S, Palberg T, Leiderer P, to be published
12. Larsen AE, Grier DG (1996) Phys Rev Lett 76:3862
13. Kepler GM, Fraden S (1994) Langmuir 10:2501
14. Pansu B, Pieranski P, Picranski P (1984) J Phys 45:331
15. Bonissent A, Pieranski P, Pieranski P (1984) Phil Mag A 50:57
16. Percus JK (1980) J Stat Phys 23:657
17. Wertheim MS, Blum L, Bratko D (1990) In: Chen S-H, Rajagopalan R (eds) Micellar Solutions and Microemulsions: Structure, Dynamics, and Statistical Thermodynamics. Springer, New York
18. Chou T, Nelson DR (1993) Phys Rev E 48:4611
19. Schmidt M, Löwen H (1996) Phys Rev Lett 76:4552
20. Hoover WG, Ree FH (1967) J Chem Phys 47:4837; see also, Frenkel D, Ladd AJC (1984) J Chem Phys 81:3188
21. Weber H, Marx D (1994) Europhys Lett 27:593; Weber H, Marx D, Binder K (1995) Phys Rev B 51:14636
22. Kirkwood JG (1950) J Chem Phys 18:380
23. Wojciechowski KW (1987) Phys Lett A 122:377
24. Schmidt M, Löwen H, to be published
25. Chang E, Hone DW (1988) J Phys 49:25
26. Löwen H (1992) J Phys Condensed Matter 4:10 105
27. Aranda-Espinoza H, Carbajal-Tinoco M, Urrutia-Banuelos E, Arauz-Lara JL, Medina-Noyola M, Alejandre J (1994) J Chem Phys 101:10 925
28. Chávez-Páez M, Méndez-Alcaraz JM, Arauz-Lara JL, Medina-Noyola M, (1996) J Coll Interface Sci 179:426
29. Chen K, Kaplan T, Mostoller M (1995) Phys Rev Lett 74:4019
30. Bagchi K, Anderson HC, Swope W (1996) Phys Rev Lett 76:255
31. Zheng L, Fertig HA (1995) Phys Rev B 52, 12282; Narasimhan S, Ho T-L (1995) Phys Rev B 52:12 291
32. Goldoni G, Peeters FM (1996) Phys Rev B 53:4591
33. Hug JE, van Swol F, Zukoski CF (1995) Langmuir 11:111
34. Courtemanche DJ, van Swol F (1992) Phys Rev Lett 69:2078; Courtemanche DJ, Pasmore TA, van Swol F (1993) Mol Phys 80:861
35. Schoen M, Diestler DJ, Cushman JH (1994) J Chem Phys 101:6865
36. For a review see: Löwen H (1994) Phys Rep 237:249
37. Rosenfeld Y, Schmidt M, Löwen H, Tarazona P (1996) J Phys Condens Matter 8:L577
38. Rosenfeld Y (1993) J Chem Phys 98:8126
39. Ohnesorge R, Löwen H, Wagner H (1994) Phys Rev E 50:4801
40. Choudhury N, Ghosh SK (1996) J Chem Phys 104:9563
41. Idziak SHJ, Koltover I, Davidson P, Ruths M, Li Y, Israelachvili JN, Safinya CR (1996) Physica B 221:289
42. Bolhuis P (1996) PhD thesis, University of Utrecht
43. Kravitz S (1967) Math Mag 40:65; (1969) U Pirl Math Nachr 40:111; Goldberg M (1971) Math Mag 44:134
44. Peikert R (1994) El Math 49:16